JVI Journals.ASM.org

The Crystal Structure of a Cardiovirus RNA-Dependent RNA Polymerase Reveals an Unusual Conformation of the Polymerase Active Site

Laia Vives-Adrian,[a,b] Celia Lujan,[a] Baldo Oliva,[c] Lonneke van der Linden,[d,e*] Barbara Selisko,[f] Bruno Coutard,[f] Bruno Canard,[f] Frank J. M. van Kuppeveld,[d,g] Cristina Ferrer-Orta,[a] Núria Verdaguer[a]

Institut de Biologia Molecular de Barcelona (CSIC), Parc Científic de Barcelona, Barcelona, Spain[a]; Enteric Virus Laboratory, Department of Microbiology, University of Barcelona, Barcelona, Spain[b]; Structural Biology Laboratory (GRIB-IMIM), Department of Experimental and Life Sciences, Universitat Pompeu Fabra, Barcelona, Spain[c]; Department of Medical Microbiology, Nijmegen Centre for Molecular Life Sciences & Nijmegen Institute for Infection, Inflammation and Immunity, Radboud University Nijmegen Medical Centre, Nijmegen, The Netherlands[d]; Laboratory of Virology and Chemotherapy, Rega Institute for Medical Research, University of Leuven, Leuven, Belgium[e]; Research Group Viral Replicases, AFMB, Universités Aix-Marseille I et II, Marseille, France[f]; Virology Division, Department of Infectious Diseases and Immunology, Faculty of Veterinary Medicine, Utrecht University, Utrecht, The Netherlands[g]

ABSTRACT

Encephalomyocarditis virus (EMCV) is a member of the *Cardiovirus* genus within the large *Picornaviridae* family, which includes a number of important human and animal pathogens. The RNA-dependent RNA polymerase (RdRp) 3D^{pol} is a key enzyme for viral genome replication. In this study, we report the X-ray structures of two different crystal forms of the EMCV RdRp determined at 2.8- and 2.15-Å resolution. The *in vitro* elongation and VPg uridylylation activities of the purified enzyme have also been demonstrated. Although the overall structure of EMCV 3D^{pol} is shown to be similar to that of the known RdRps of other members of the *Picornaviridae* family, structural comparisons show a large reorganization of the active-site cavity in one of the crystal forms. The rearrangement affects mainly motif A, where the conserved residue Asp240, involved in ribonucleoside triphosphate (rNTP) selection, and its neighbor residue, Phe239, move about 10 Å from their expected positions within the ribose binding pocket toward the entrance of the rNTP tunnel. This altered conformation of motif A is stabilized by a cation-π interaction established between the aromatic ring of Phe239 and the side chain of Lys56 within the finger domain. Other contacts, involving Phe239 and different residues of motif F, are also observed. The movement of motif A is connected with important conformational changes in the finger region flanked by residues 54 to 63, harboring Lys56, and in the polymerase N terminus. The structures determined in this work provide essential information for studies on the cardiovirus RNA replication process and may have important implications for the development of new antivirals targeting the altered conformation of motif A.

IMPORTANCE

The *Picornaviridae* family is one of the largest virus families known, including many important human and animal pathogens. The RNA-dependent RNA polymerase (RdRp) 3D^{pol} is a key enzyme for picornavirus genome replication and a validated target for the development of antiviral therapies. Solving the X-ray structure of the first cardiovirus RdRp, EMCV 3D^{pol}, we captured an altered conformation of a conserved motif in the polymerase active site (motif A) containing the aspartic acid residue involved in rNTP selection and binding. This altered conformation of motif A, which interferes with the correct positioning of the rNTP substrate in the active site, is stabilized by a number of residues strictly conserved among picornaviruses. The rearrangements observed suggest that this motif A segment is a dynamic element that can be modulated by external effectors, either activating or inhibiting enzyme activity, and this type of modulation appears to be general to all picornaviruses.

The *Picornaviridae* family is one of the largest virus families known and includes many important human and animal pathogens, such as polioviruses (PV), human rhinoviruses (HRV), and foot-and-mouth disease virus (FMDV) (1, 2). The *Cardiovirus* genus consists of two species: encephalomyocarditis virus (EMCV) and related viruses (mengovirus, Columbia SK virus, and Maus-Elberfeld virus) (3) and *Theilovirus* (4–6). All of these viruses infect rodents, replicate in the gastrointestinal tract, and are transmitted by the fecal-oral route. Although rodents are the natural reservoir of these viruses, EMCV has also been isolated from many other hosts, including various mammals, birds, and invertebrates (7, 8). Infection of other mammalian species by EMCV is often fatal and associated with outbreaks of myocarditis and encephalitis. Human EMCV infection and associated disease have been documented, but clinical manifestation is probably infrequent (1). *Theilovirus* species are classified into five types, two of which infect humans: Vilyuisk human encephalomyelitis virus and Saffold virus (9, 10). Recently, several new types of Saffold

Received 29 November 2013 **Accepted** 26 February 2014

Published ahead of print 5 March 2014

Editor: W. I. Sundquist

Address correspondence to Cristina Ferrer-Orta, cfocri@ibmb.csic.es, or Núria Verdaguer, nvmcri@ibmb.csic.es.

* Present address: Lonneke van der Linden, Department of Medical Microbiology, Laboratory of Clinical Virology, Academic Medical Center, University of Amsterdam, Amsterdam, The Netherlands.

Copyright © 2014, American Society for Microbiology. All Rights Reserved.

doi:10.1128/JVI.03502-13

Downloaded from http://jvi.asm.org/ on March 26, 2015 by Universiteitsbibliotheek Utrecht

virus were isolated from young children with upper respiratory symptoms or gastroenteritis (11, 12; reviewed in reference 8).

The picornaviral RNA-dependent RNA polymerase (RdRp) $3D^{pol}$, responsible for RNA genome replication, has been extensively studied, and there is a growing body of information available on $3D^{pol}$ structure and function. To date, the crystal structures of RdRps for six different members of the enterovirus genus and for the aphthovirus FMDV have been reported either isolated or bound to different substrates (13–23). These enzymes adopt the classical closed right-hand architecture, having finger, palm, and thumb subdomains, with fingertips anchored on the thumb generating an encircled active site. Seven motifs (A to G) conserved in sequence and structure have been defined that play critical roles in recognition and binding of nucleoside triphosphates (A, B, D, and F), metal ion binding and phosphoryl transfer (A and C), structural integrity of the palm (D), priming nucleotide binding (E), and template binding (B, F, and G) (reviewed in references 24 and 25).

Mutational and structural analyses in PV also have demonstrated that some substitutions in residues located far from the active site, in particular at the polymerase N terminus, have significant effects on catalysis (14). In addition, a number of mutant polymerases that show altered polymerization fidelity have been identified harboring mutations remote from the active site (26–28). All of these observations suggest that nucleotide binding and incorporation are modulated by a long-distance network of interactions (14, 29–32).

To gain insight into the elucidation of the dynamics-function relationships in RdRps, we have solved the crystal structure of the first cardiovirus RdRp, the EMCV $3D^{pol}$, in two different crystal forms at 2.15-Å and 2.8-Å resolution. Interestingly, in one of the crystal forms, we captured an unusual conformation of motif A, occupying the rNTP channel entry. In this conformation, motif A directly interacts with a conserved lysine in the finger domain and with motif F. The structure also shows that the first residue, Gly1, is moved out of its binding pocket, buried in the finger domain, toward an exposed orientation in the polymerase surface. Finally, we have also demonstrated that the recombinant enzyme is active *in vitro* for both VPg uridylylation and RNA elongation.

MATERIALS AND METHODS

Protein expression and purification. The genomic region coding for the RNA-dependent RNA polymerase 3D of encephalomyocarditis virus, type mengovirus (EMCV $3D^{pol}$), derived from infectious clone pM16.1 (33), was cloned into the expression plasmid pETG20A Gateway (Invitrogen). This plasmid provides a six-histidine tag attached at the carboxyl terminus of the protein which can be removed by digestion with tobacco etch virus (TEV) protease (Invitrogen).

Protein was produced in *Escherichia coli* Rosetta (DE3) pLysS strain. Transformed cells were grown in Turbo Broth medium (AthenaES) supplemented with 100 $\mu g\ ml^{-1}$ ampicillin and 34 $\mu g\ ml^{-1}$ chloramphenicol at 310 K until an optical density at 600 nm (OD_{600}) of 0.4 to 0.6 was reached, and then the solution was tempered to 293 K. Expression was induced with 500 μM isopropyl-ß-D-thiogalactopyranoside (IPTG) for 16 h at 293 K. Cells were pelleted by centrifugation at 4,500 × *g* for 30 min and then resuspended in 40 ml of phosphate-buffered saline (PBS; 1×). Finally, cells were harvested by centrifugation and stored at −80°C.

Cells were resuspended in a cold lysis buffer containing 50 mM Tris-HCl, pH 8.0, 500 mM NaCl, 10 mM imidazole, 0.1% (vol/vol) Triton X-100, 10% glycerol, 1 mg ml^{-1} lysozyme, and 10 $\mu g\ ml^{-1}$ DNase and lysed by sonication. Cellular debris were pelleted by centrifugation, and the soluble fraction was filtered and loaded into a 5-ml HisTrap HP (GE Healthcare). Elution was carried out with an imidazole gradient (10 to 500 mM) in 50 mM Tris, pH 8.0, 500 mM NaCl, 10% glycerol, and 1 mM dithiothreitol (DTT). Fractions containing the protein were dialyzed against 50 mM Tris, pH 8.0, 300 mM NaCl, 10% glycerol, and 1 mM DTT. His tag was removed by a digestion with TEV protease (Invitrogen) at 293 K for 16 h. Both the His tag and TEV protease were removed by running a second Ni affinity chromatography. Finally, fractions containing the protein were further purified by size exclusion on a Superdex 200 16/60 (GE Healthcare) in 500 mM NaCl, 50 mM Tris-HCl, pH 8.0, 10% glycerol, 1 mM DTT, and 1 mM EDTA. The protein was concentrated to 10 mg ml^{-1} using an Amicon Ultra concentrator (10,000 molecular weight cutoff polyethersulfone [PES]; Millipore) previously equilibrated with a protein buffer containing 50 mM arginine and 50 mM glutamine (Sigma-Aldrich). The protein was stored at 193 K and the purity grade analyzed by SDS-PAGE.

For the biochemical activity assays, the EMCV $3D^{pol}$ was expressed at 17°C in Turbest broth (Arcadia Biotech). Protein purification and tag removal were performed under nondenaturing conditions as previously described (34). The final size-exclusion chromatography step was performed in 10 mM HEPES, 300 mM NaCl, 2 mM DTT, pH 7.5.

Polymerase activity assays. The polymerase elongation activity assays were performed as described previously (16). Starting conditions for filter-binding polymerase activity assays optimized for coxsackievirus B3 (CVB3) $3D^{pol}$ were conducted in a mix of 50 μl containing 50 mM Tris, pH 7.0, 10 mM KCl, 0.8 mM $MgCl_2$, 9% glycerol, 2 μM oligo(dT_{15}) (Invitrogen) annealed to 350 nM poly(rA) [termed poly(rA)/dT15; average size, 519 nucleotides (nt); oligo$(dT)_{15}$/poly(rA) molar ratio of 5.7:1; GE Healthcare], 40 nM EMCV $3D^{pol}$, 10 μM UTP, and 0.5 μCi [^{3}H]UTP (35.5 Ci/mmol; GE Healthcare). Final conditions obtained for EMCV $3D^{pol}$ were 50 mM morpholine propanesulfonic acid (MOPS), pH 7.0, 10 mM KCl, 4 mM $MgCl_2$, 9% glycerol, 2 μM oligo(dT_{15}) annealed to 350 nM poly(rA), 0.5 μM EMCV $3D^{pol}$, 100 μM UTP, and 2 μCi [^{3}H]UTP.

Visualization of elongation products by denaturing PAGE was carried out as described previously (16). The same reaction mixture was used as described above, except that [^{32}P]UTP (10 μCi) was used instead of [^{3}H]UTP. Ten-μl samples were taken at 0, 10, 20, and 30 min.

VPg uridylylation reactions were performed as described previously (16). The reaction mix for EMCV $3D^{pol}$ contained 50 mM HEPES, pH 8.0, 10 mM KCl, 1 mM $MnCl_2$, 9% glycerol, 2 μM poly(rA), 150 μM EMCV VPg (GPYNETTRIKPKTLQLLDVQ; Perbio Science, France), 2 μM EMCV $3D^{pol}$, 5% dimethylsulfoxide (DMSO), 100 μM UTP, and 20 μCi [^{32}P]UTP. Fifteen-μl samples were taken at 0, 60, and 120 min and analyzed by Tris-tricine SDS-PAGE.

Crystallization. Initial crystallization trials of EMCV $3D^{pol}$ were performed by the sitting-drop vapor diffusion method at both 277 and 293 K in 96-well Greiner plates using a nanoliter-drop crystallization robot (Cartesian Microsys 4000 XL) and the commercial screens: crystal screens 1 and 2 and salt RX (Hampton research). Protein solution (10 mg ml^{-1} in 500 mM NaCl, 50 mM Tris-HCl, pH 8.0, 10% glycerol, 1 mM DTT, and 1 mM EDTA) droplets of 100 nl were mixed with 100 nl of precipitant solution; the reservoir volume was 100 μl. Two different crystal forms were obtained. The first crystals appeared in 1 day at 277 K from a solution containing 10% polyethylene glycol (PEG) 6,000 and 2.0 M NaCl. These crystals were optimized in the same plates using the Cartesian robot but increasing the drop volume to 400 nl (200 nl protein solution and 200 nl crystallization buffer). The second crystal form was optimized at 293 K in a 24-well Greiner plate in crystallization drops containing 1 μl of protein solution and 1 μl of crystallization buffer (4.0 M ammonium acetate and 0.1 M sodium acetate, pH 4.6) equilibrated against 1 ml of crystallization buffer. Crystals appeared in 4 or 5 days.

X-ray diffraction analysis. EMCV $3D^{pol}$ data sets were collected at the ALBA-CELLS synchrotron light facility (Barcelona) on a Pilatus 6M Dectris detector at beamline XALOC (λ = 0.979 Å). All of the data sets were recorded at 100 K. The first crystal form, belonging to the $I4_122$ space group, diffracted to 2.15-Å resolution (Table 1). Two hundred images

Downloaded from http://jvi.asm.org/ on March 26, 2015 by Universiteitsbibliotheek Utrecht

TABLE 1 Data collection and refinement statistics

Parameter	Value(s) for crystal form:	
	$I4_122$	C2
Data collection statistics		
Resolution range (Å)	43.15–2.15 (2.27–2.15)	49.32–2.8 (2.95–2.8)
Space group	$I4_122$	C121
Cell dimensions		
a, *b*, *c* (Å)	122.55, 122.55, 198.79	230.40, 140.77, 170.58
α, β, γ (°)	90, 90, 90	90, 125.86, 90
R_{merge}	0.09 (0.77)	0.05 (0.56)
$I/\sigma I$	13.1 (2.8)	10.2 (1.8)
Completeness (%)	98.4 (98.3)	98.9 (99.2)
Multiplicity	5.0 (5.0)	2.3 (2.3)
Refinement statistics		
Resolution range (Å)	43.15–2.15	48.97–2.8
No. reflections (total/unique)	201,287/40,499	250,575/107,270
R_{work}[a]/R_{free}[b]	23.89/26.30	21.51/25.11
No. of residues		
Protein	460	2760
Ligands	2 glycerol, 1 Gln[c]	7 glycerol
Water	105	123
B factor (Å^2)		
Protein	27.30	53.16
Water + ligands	37.12	43.80
RMSD		
Bond length (Å)	0.004	0.006
Bond angle (°)	0.887	1.05
Ramachandran plot (no. [%])		
Residues in preferred regions	439 (95.9)	2,544 (92.85)
Residues in allowed regions	15 (3.3)	137 (5.0)

[a] $R_{work} = \sum hkl ||F_{obs}(hkl)| - |F_{calc}(hkl)|| / \sum hkl |F_{obs}(hkl)|$, where F_{obs} and F_{calc} are the structure factors deduced from measured intensities and those calculated from the model, respectively.

[b] R_{free} is the same as R_{work} but was determined for 5% of the total reflections chosen at random and omitted from refinement.

[c] The Gln molecule was present in the buffer used for washing the concentrator membranes to improve protein solubility and prevent membrane binding.

were collected with an oscillation angle of 0.5° and 1-min exposure time as a collection strategy. The second crystal form, belonging to the space group C2 and with six independent RdRp molecules present in the asymmetric unit, diffracted to 2.8-Å resolution (Table 1). Four hundred images were collected from these crystals, with an oscillation angle of 0.5° and an oscillation time of 1 min. Diffraction images were processed with XDS (35) and internally scaled with SCALA (CCP4i) (36).

Structure solution and refinement. In both space groups, the structure of the EMCV 3D^{pol} was determined by molecular replacement with PHENIX software (37) using a search model derived from the structure of FMDV polymerase (Protein Data Bank [PDB] entry 1U09). The correctly oriented and positioned models were manually rebuilt using Coot (38) and automatically refined with Refmac5 (39) for the $I4_122$ structure; Refmac5 and PHENIX were used for the C2 structures. Noncrystallographic symmetry (ncs) restraints were initially applied to the six independent molecules present in the asymmetric unit of the C2 crystals using Refmac5. However, the ncs restrained-refinement result was unstable because the presence of different conformations in many polymerase regions, especially in the surface-exposed loops, was affected by crystal-packing interactions. Therefore, the variable regions were manually rebuilt using Coot, and the final cycles of automatic refinement were performed with PHENIX. The refined structures in both space groups contain the complete protein residues (from Gly1 to Trp460). The C2 structure also contains 7 glycerol molecules and 123 water molecules, and the $I4_122$ structure contains 2 glycerol molecules and 105 water molecules (Table 1). In addition, an elongated extra density, present in the active-site cavity of the $I4_122$ crystal form, has been interpreted according to the presence of a glutamine molecule from the buffer used for washing the concentrator membranes prior to protein concentration (40). The statistics of the refinement for the two structures are summarized in Table 1.

Structural analysis. The knowledge-based potentials of the program Prosa2003 (41) were used to compare the quality of the structures. Prosa potentials are based on the use of the inverse of the Boltzmann equation, inferring the energy of a system based on the frequency with which pairs of residues are found at a given distance in the Protein Data Bank. The total energy is split into two main components: pair energy, which checks the quality of the residue-residue interactions, and surf energy, to check the residue interaction with the solvent. The quality of the whole structure is evaluated by means of the Z score [Z score = $(E - <E>)/s$, where E is the energy of a particular conformation, $<E>$ is the average of energies obtained with the sequence tested in all possible folds stored in Prosa, and s is the standard deviation of the test]. The combined (comb) Z score for surf energy and pair energy potentials for the EMCV 3D^{pol} structures yielded identical values for both standard and altered conformations of motif A (Z score [comb] = −13.5), with subtle differences in the individual surf and pair energies calculated (Z-score [surf] = −10.03 and Z-score [pair] = −10.45 for the standard conformation; Z-score [surf] = −9.92 and Z-score [pair] = −10.64 for the altered conformation). These values were within the expected range for a protein of 460 residues (Prosa Manual; http://www.came.sbg.ac.at), indicating that both standard and altered conformations were stable.

However, these energy calculations are not enough to ensure that the conformation of a sequence in a particular fold is the best. To further check the local differences in stability between the two motif A loop conformations, a new analysis was performed taking into account only the residues of the motif A loop (237 to 243), the closest contacting zone that included the region of residues 50 to 64 and residue 1. Calculations were done by scanning the sequence of these regions with all possible amino acid substitutions. The Z-score of the new structure was calculated and compared to the Z-score of the original (nonmutated) sequence. The results obtained are summarized in Table 2.

PDB accession numbers. The PDB accession codes for the EMCV 3D^{pol} structures are 4NYZ and 4NZ0 for $I4_122$ and C2 crystal forms, respectively.

RESULTS

***In vitro* polymerase activity of recombinant EMCV 3D^{pol}.** Polymerase activity of the purified EMCV 3D^{pol} was assayed by measuring elongation of an oligo(dT_{15}) primer hybridized to a poly(rA) template through incorporation of [^{3}H]UTP. Negligible elongation activity could be observed when using conditions optimized for CVB3 3D^{pol} {50 mM Tris buffer, pH 7.0, 0.8 mM $MgCl_2$, 40 nM 3D^{pol}, 9% glycerol, 10 μM UTP, 0.01 μCi/μl [^{3}H]UTP, 2 μM oligo(dT_{15}) annealed to 350 nM poly(rA); L. van der Linden, L. Vives-Adrián, B. Selisko, C. Ferrer-Orta, H. Venselaar, K. Lanke, A. M. De Palma, F. Tanchis, N. Goris, D. Lefebvre, K. De Clercq, P. Leyssen, C. Lacroix, G. Pürstinger, R. Ulferts, B. Coutard, B. Canard, N. Verdaguer, J. Neyts, and F. J. M. van Kuppeveld, unpublished data}. Therefore, the assay was optimized for EMCV 3D^{pol} using conditions described for FMDV 3D^{pol} (42), an enzyme with a higher similarity to EMCV 3D^{pol} than CVB3 3D^{pol}, as a guideline. A higher enzyme concentration (0.4 to 1 μM compared to 40 nM for CVB3 3D^{pol}) was required to observe some activity (data not shown). The change to MOPS buffer (pH 7.0) instead of Tris (pH 7.0) was decisive (Fig. 1A). This was also the

Downloaded from http://jvi.asm.org/ on March 26, 2015 by Universiteitsbibliotheek Utrecht

TABLE 2 Pseudoenergies of selected residues of $I4_122$ and C2 EMCV $3D^{pol}$ conformations[a]

Residue		Surface energy						Pair energy						Combined energy					
		$I4_122$			C2			$I4_122$			C2			$I4_122$			C2		
No.	Identity	$\Delta < 0$	$\Delta > 0$	I	$\Delta < 0$	$\Delta > 0$	I	$\Delta < 0$	$\Delta > 0$	I	$\Delta < 0$	$\Delta > 0$	I	$\Delta < 0$	$\Delta > 0$	I	$\Delta < 0$	$\Delta > 0$	I
1	G	0	19		17	2	+	3	16		1	18		1	18		11	8	
50	D	2	17		17	2	+	2	17		0	19		0	19		5	14	
51	E	1	18		1	18		1	18		1	18		0	19		1	18	
52	V	5	14		14	5		4	15		3	16		4	15		10	9	
53	A	6	13		9	10		0	19		4	15		4	15		5	14	
54	F	0	19		0	19		4	15		9	10		1	18		0	19	
55	S	6	13		3	16		8	11		6	13		5	14		1	18	
56	K	16	3	+	16	3	+	3	16		2	17		11	8		15	4	+
57	H	9	10		9	10		6	13		6	13		9	10		4	15	
58	T	0	19		0	19		1	18		1	18		1	18		0	19	
59	S	2	17		2	17		1	18		1	18		3	16		1	18	
60	N	13	6		13	6		7	12		4	15		14	5		12	7	
61	Q	14	5		14	5		7	12		13	6		15	4	+	16	3	+
62	E	1	18		4	15		7	12		5	14		12	7		5	14	
63	T	9	10		9	10		12	7		5	14		8	11		6	13	
64	L	2	17		2	17		0	19		0	19		0	19		0	19	
237	S	16	3	+	6	13		3	16		1	18		11	8		2	17	
238	N	12	7		12	7		1	18		2	17		4	15		11	8	
239	F	0	19		0	19		12	7		15	4	+	3	16		3	16	
240	D	2	17		18	1	+	0	19		12	7		0	19		19	0	+
241	S	16	3	+	12	7		1	18		5	14		11	8		12	7	
242	T	11	8		11	8		4	15		8	11		11	8		12	7	
243	H	9	10		9	10		3	16		3	16		7	12		7	12	

[a] Mutability analysis was performed to characterize the stability of the motif A loop (residues 237 to 243) and the surrounding selected residues (50 to 64 and 1). The analysis consists of the replacement of each residue by all other 19 amino acids. The Z-score of the structure then is calculated by Prosa and compared to the Z-score of the original (nonmutated) sequence. We used Z-scores of pair, surface, and combined energies. Columns show the number of mutations stabilizing ($\Delta < 0$) and destabilizing ($\Delta > 0$) the standard conformation of EMCV $3D^{pol}$ pseudoenergies. Δ is the difference between the mutated residue and initial residue energies. By convention, we assumed that when $\Delta < 0$ is greater than 15, a significant unstable localization of the conformation occurred. Column I shows a plus mark when the mutations stabilize the conformation in a particular position. Rows show the selected residues for this analysis.

buffer used in elongation assays with FMDV $3D^{pol}$ (42). On the other hand, decreasing the glycerol concentration from 9% to 2.5% was detrimental to EMCV $3D^{pol}$ elongation activity. The increase of cofactor $MgCl_2$ concentration (3 to 5 mM $MgCl_2$ compared to 0.8 to 1 mM) resulted in significantly improved elongation activity (Fig. 1C). Using 1 mM $MnCl_2$ resulted in only a small increase in activity and was abandoned in favor of the more physiological ion $MgCl_2$. We also checked the influence of UTP concentration. Using 10, 50, or 100 μM UTP yielded similar apparent incorporation rates of [^{3}H]UTP (Fig. 1C). However, considering that the labeled UTP is diluted more when using a higher concentration of unlabeled UTP, the outcome observed with 100 μM UTP represents a higher level of elongation activity; thus, 100 μM UTP was selected. Using optimized conditions, elongation product formation by EMCV $3D^{pol}$ followed linear kinetics up to 30 min (Fig. 1D). Resulting polymerase elongation products could be visualized by PAGE, showing time-dependent formation of an oligo(dT_{15})-poly(rU) product in a highly processive manner (Fig. 1E). Furthermore, we could also show uridylylation of the physiological $3D^{pol}$ primer VPg by $3D^{pol}$ in an assay using purified VPg and a poly(rA) template (Fig. 1E).

In summary, we demonstrate that recombinant EMCV $3D^{pol}$ is active as a processive primer-dependent, RNA-dependent RNA polymerase *in vitro*. We also showed that it uridylates its cognate VPg primer.

Overall architecture of the ECMV RdRp. Two different crystal forms, space groups $I4_122$ and C2, were obtained from the EMCV $3D^{pol}$ (Table 1; also see Materials and Methods). The C2 crystals diffracted to 2.8-Å resolution and contained six independent polymerase molecules in the asymmetric unit (a.u.), whereas the tetragonal $I4_122$ crystals diffracted to 2.15 Å and contained only one molecule per a.u. The structures were solved by molecular replacement using a homology model based on the structure of the FMDV $3D^{pol}$ (PDB entry 1U09) as a search model. Data collection and refinement statistics are summarized in Table 1.

EMCV $3D^{pol}$ adopts the classical right-hand conformation of RdRps with the N terminus, finger, and thumb subdomains interacting to encircle the active site (Fig. 2A). In the C2 crystals, the six independent polymerase molecules show similar conformations (the root mean square deviation [RMSD] between all Cα atoms is 0.5 Å). The main differences are located at the polymerase N terminus, residues 41 to 64, and in the palm loops, residues 292 to 297 and 360 to 368, at the N and C termini of motifs B and D, respectively (Fig. 2C). Subtle differences are also seen in the region of residues 440 to 448, joining the thumb helices α14 and α15. With the exception of the motif B loop, all of the residues mentioned above belong to surface-exposed regions involved in crystal-packing interactions in some of the molecules of the crystal asymmetric unit. Five of the six $3D^{pol}$-independent molecules found in this crystal form show the first residue, Gly1, buried in the finger domain, participating in a network of hydrogen bonds that connects the fingers with the motif A residue Asp240 in the

Downloaded from http://jvi.asm.org/ on March 26, 2015 by Universiteitsbibliotheek Utrecht

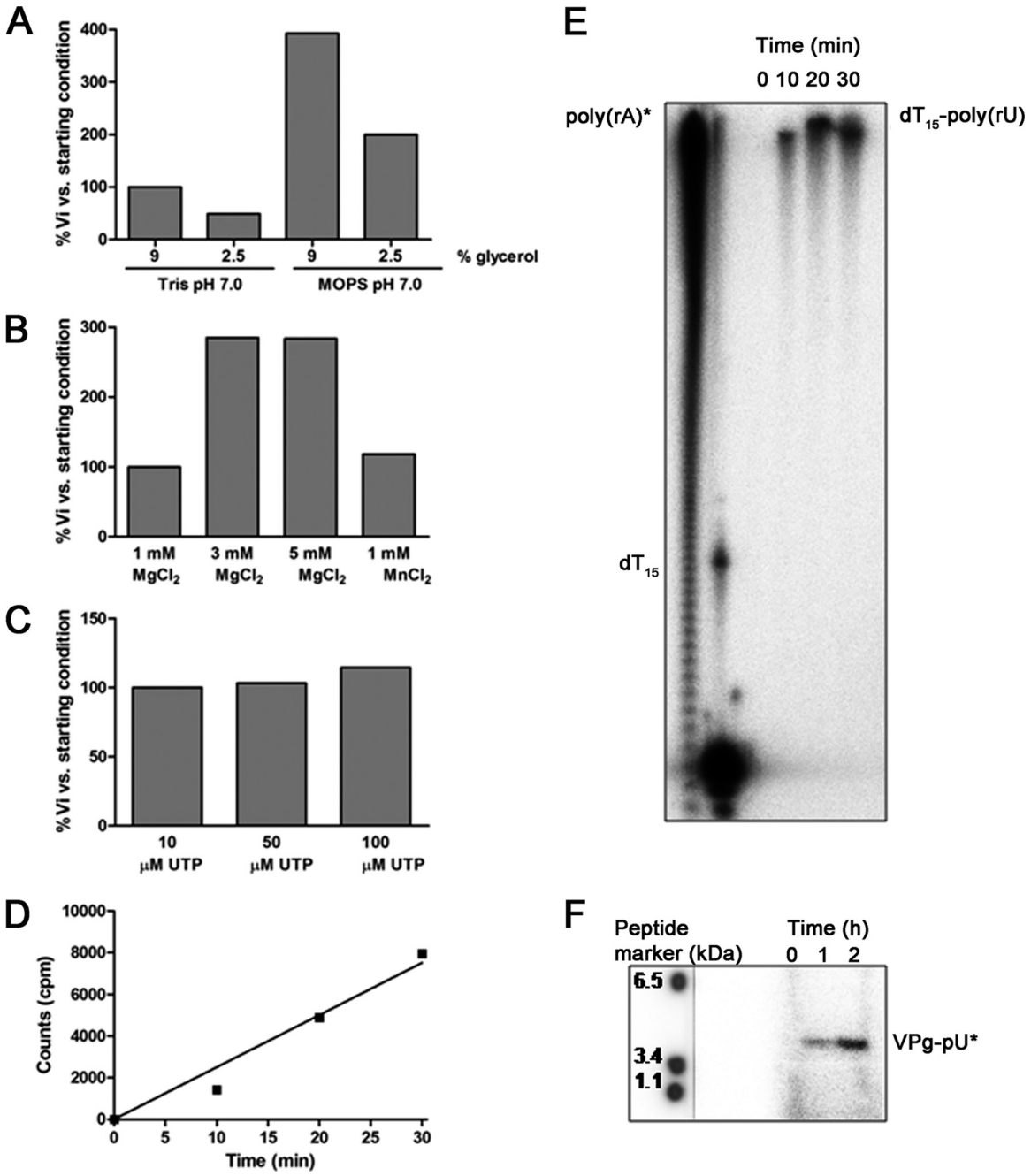

FIG 1 *In vitro* polymerase activity of EMCV 3D^{pol}. (A to D) *In vitro* EMCV 3D^{pol} elongation activity measuring incorporation of [^{3}H]UTP using poly(rA)/dT$_{15}$ as the template-primer. (A to C) Elongation activity of EMCV 3D^{pol} while varying cofactor $MgCl_2$/$MnCl_2$, UTP, and glycerol concentrations and the type of buffer. The initial velocity of the reaction (Vi) represents the polymerase elongation activity. The Vi observed with the starting conditions for the optimization was set to 100%. (D) Elongation activity of EMCV 3D^{pol} using the optimized conditions. (E) EMCV 3D^{pol} elongation activity as visualized by denaturing PAGE. The dT$_{15}$ primer is elongated with ([^{32}P])UTP using a poly(rA) template. (F) VPg uridylylation assay. In the presence of a poly(rA) template, [^{32}P]UTP is covalently coupled to the primer VPg by EMCV 3D^{pol}. Reaction products were analyzed using Tris-tricine-SDS-PAGE.

active site, as reported for all other picornaviral 3D^{pol} structures determined to date (Fig. 3A and B). However, in the sixth molecule, the Gly1 binding residues Thr58 and Asn60 are reoriented and participate in packing contacts with a neighboring molecule in the crystal, leaving Gly1 in a partially exposed position (Fig. 3C). This glycine is clearly visible in the electron density maps, and its position is probably stabilized by a salt bridge created between the Gly1 N terminus and the side chain of Glu4 (Fig. 3C).

As for the other picornaviral RdRps, the EMCV 3D^{pol} fingers are divided into two regions: an inner region that consists primarily of a bundle of α-helices (from α1 to α4 and α6, α8, and α9), packed against the palm subdomain, and an outer region, consisting of a five-stranded mixed β-sheet (β1, β5, β7, β9, and β10), with strand β1 contributed from the N terminus. The long region connecting strands β5 and β7 (residues 151 to 179) contains two small secondary structural elements, α5 and β6, which, together

Downloaded from http://jvi.asm.org/ on March 26, 2015 by Universiteitsbibliotheek Utrecht

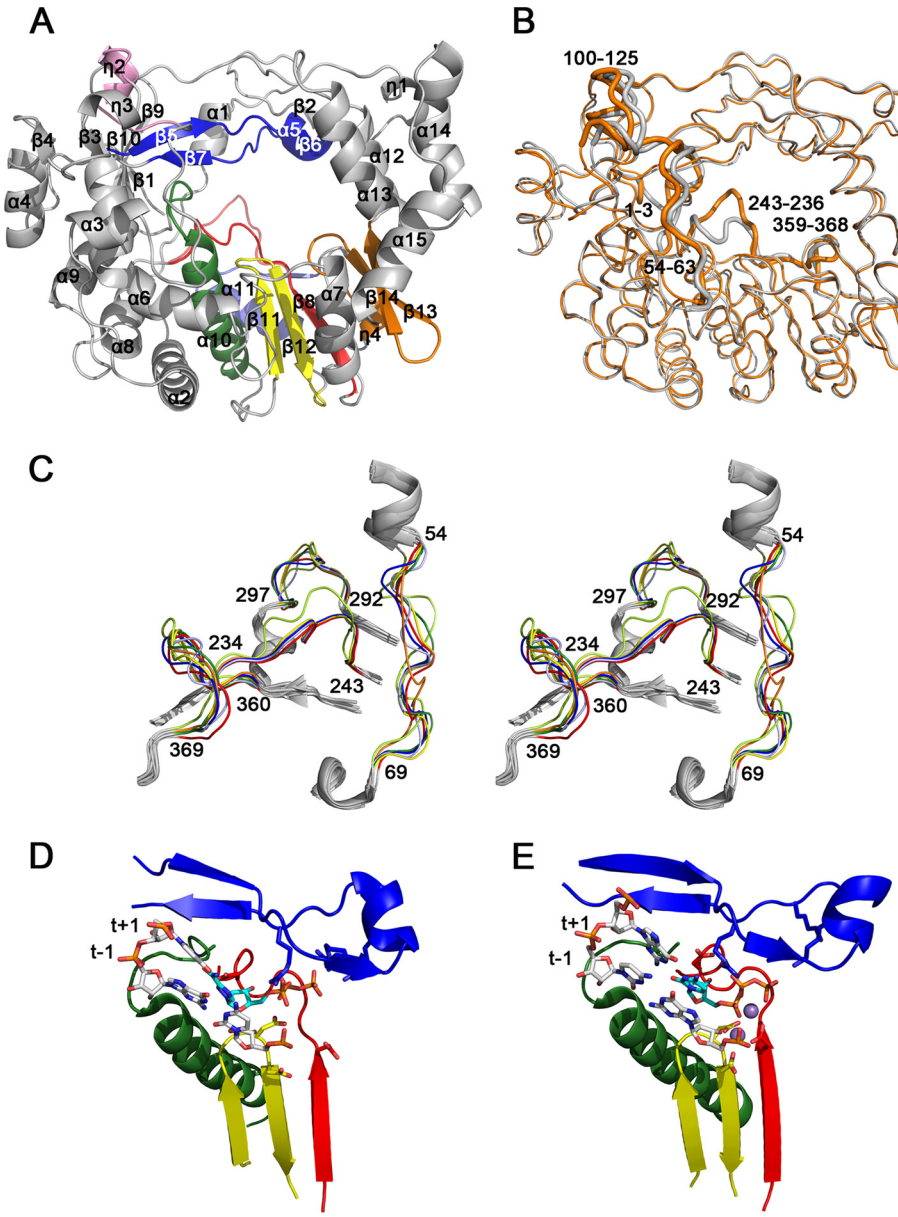

FIG 2 Structure of EMCV 3D^{pol}. (A) Front view of the EMCV 3D^{pol} structure, showing a ribbon diagram (gray) with the secondary structural elements explicitly labeled. The seven conserved structure-sequence motifs are colored according to the following scheme: A, red; B, green; C, yellow; D, light blue; E, orange; F, blue; and G, pink. (B) Superimposition of the EMCV 3D^{pol} structures in the C2 (gray) and $I4_122$ (orange) space groups. The polymerase regions showing the largest displacements are highlighted with thicker ribbons and labeled. (C) Stereo view of the closeup of the seven EMCV 3D^{pol} structures solved by superimposition, viewed from the back of the enzyme. The panel shows the palm motif A (residues 234 to 243), the B-loop (residues 292 to 297), and motif D (residues 360 to 369), highlighting the largest movements in different colors. The region between residues 54 and 69 of the fingers that contacts motif A is also represented. Panels D and E show the active-site closure in RdRps upon correct nucleotide binding. (D) Ribbon diagram of the palm subdomain of the FMDV 3D^{pol}-RNA-RTP ternary complex (PDB entry 2E9R). The structure was trapped in an initial precatalytic step, where the polymerase active site shows an open conformation characterized by a partially formed three-stranded β-sheet of motifs A and C. (E) Norovirus RdRp-RNA-rNTP ternary complex trapped in a catalytically competent closed conformation, where the β-strand structure of motif A was completely formed (PDB entry 3BSO). In the two panels, motifs A, B, C, and F are indicated in red, green, yellow, and blue, respectively. The template-primer RNAs and the incoming NTPs are included in both catalytic complexes. Panel E shows the two metal ions as purple balls.

with the 3_{10} helix η1 and the strand β2 at the N terminus, extend toward the thumb domain, forming the fingertip region (Fig. 2A). The long β5-β7 loop also contains the conserved motif F, which is rich in positively charged residues that form the roof of the rNTP entry channel (Fig. 2A). These residues bind the incoming rNTP and also assist the reorientation of its triphosphate moiety in the correct position for catalysis, as seen in the structures of enterovirus and aphthovirus catalytic complexes (17, 19). Finally, at the front side of the fingers, the long loop connecting helices α3 and η2 (residues 98 to 120) contains motif G (residues 110 to 120), which forms the template channel entrance (Fig. 2A).

The palm domain of EMCV 3D^{pol} consists of the central three-

Downloaded from http://jvi.asm.org/ on March 26, 2015 by Universiteitsbibliotheek Utrecht

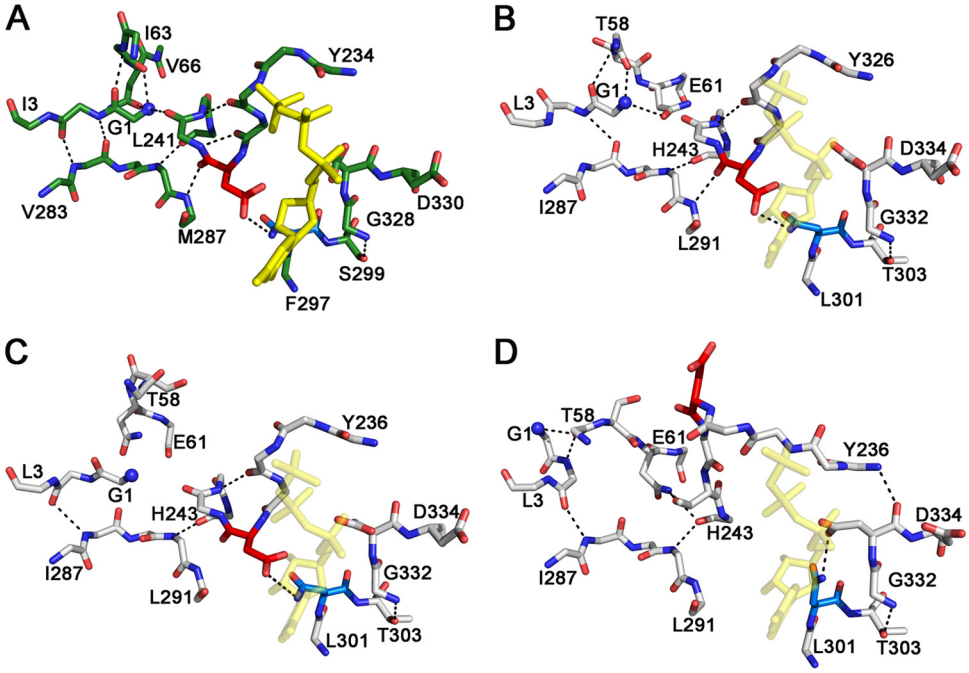

FIG 3 Network of interactions linking the polymerase N terminus to the active site in different 3D^{pol} structures. (A) PV 3D^{pol} bound to an rNTP molecule shown in yellow (PDB entry 1RA6); (B) EMCV C2 crystals, representative structure of five of the six independent molecules in the asymmetric unit; (C) EMCV C2 crystals, sixth molecule; (D) EMCV $I4_122$ crystals. In all panels, the polymerase residues are shown as sticks in atom type code, with the motif A Asp highlighted in red and the motif B Asn shown in blue. The rNTP found in the PV structure is modeled in EMCV structures by superposition of the active-site residues and represented in semitransparent yellow sticks.

stranded β-sheet (β8, β11, and β12) sandwiched between helices α7 and α11 and followed by a pair of β-strands (β13 and β14) which form the interface with the mostly helical thumb (Fig. 2A). Strand β8 and its C-terminal loop contain the conserved acidic residues Asp235 and Asp240 and form motif A. Motif C is located in the β11-β12 turn and contains the sequence Gly332-Asp333-Asp334, which is almost universally conserved in RdRps. The metal ions involved in the nucleotidyl transfer reaction would interact with the N-terminal aspartic acid residues of both A and C motifs. The helix α10 packs adjacent to the central β-sheet near the catalytic site. This helix, together with its N-terminal loop (the β10-α10 loop), forms motif B. The B-loop contains the strictly conserved residues Gly289, Ser293, Gly294, and Thr298, which are involved in binding the template (t + 1, the templating nucleotide located just in front of the incoming nucleotide) and incoming nucleotides (Fig. 2D and E; also see Fig. 5A and B), in the structures of the different picornaviral catalytic complexes determined (17–19, 43). The helix α10 also contains the conserved Asn302, which, together with Asp240 in motif A, has been described to be essential for selection of rNTPs over deoxynucleoside triphosphates (dNTPs) by hydrogen bonding to the 2′ hydroxyl group of the incoming nucleotide. In the six independent RdRp structures seen in the C2 crystals, Asn302 appears to be hydrogen bonded to Asp240 (Fig. 3B and C), as in other picornaviral RdRp structures. The helix α11 supports the central (β8, β11, and β12) sheet and, together with the long loop at its C terminus (α11-β13 loop), forms motif D. The transition between palm and thumb subdomains is provided by the two antiparallel β-strands (β13 and β14), forming the structural motif E (Fig. 2A).

In common to all other picornaviral RdRps, EMCV 3D^{pol} possesses a small thumb subdomain, built mainly by helices α12 to α15, organized in a four helix-bundle (Fig. 2A). The small size of this domain contributes to the formation of the large central cleft, located in the front of the molecule, that is typical of primer-dependent RdRps (21, 43, 44). The end of the C-terminal helix α15 is anchored to the palm domain via hydrophobic interactions between Phe459 and Val216 of helix α7 and Leu390 in the turn of motif E. The most C-terminal residue, Trp460, appears exposed to the solvent and participates in interactions with neighboring 3D^{pol} molecules in the crystal. Mutational studies in mengovirus indicated that a deletion of Trp460 or its replacement by Ala or Phe dramatically impaired viral RNA replication. The study also showed that replacement of this Trp by Tyr or His did not alter viral growth. In light of these data, the authors suggested that Trp460 is involved in thumb-palm contacts via a hydrophobic interaction with Val216 and a polar bond with the side chain of Thr219 (45). The structures of the seven independent molecules analyzed in this work show that the residue mediating thumb-palm interactions is Phe459, and that Trp460 is exposed to the solvent or participates in packing interactions with neighbor molecules. In particular, Trp460 was found in contact with Arg21 of a neighboring 3D^{pol} in two of the six independent molecules of the C2 crystal form. Therefore, the structural data indicate that the critical role of Trp460 in cardiovirus replication is due to its implication in interactions with other molecules within the replication complex.

Unusual conformation of motif A unveiled from the $I4_122$ crystal form. The overall 3D^{pol} structures observed in the two different space groups also agree very well (RMSD of 1.1 Å) (Fig. 2B). However, an important distortion of the polymerase active

Downloaded from http://jvi.asm.org/ on March 26, 2015 by Universiteitsbibliotheek Utrecht

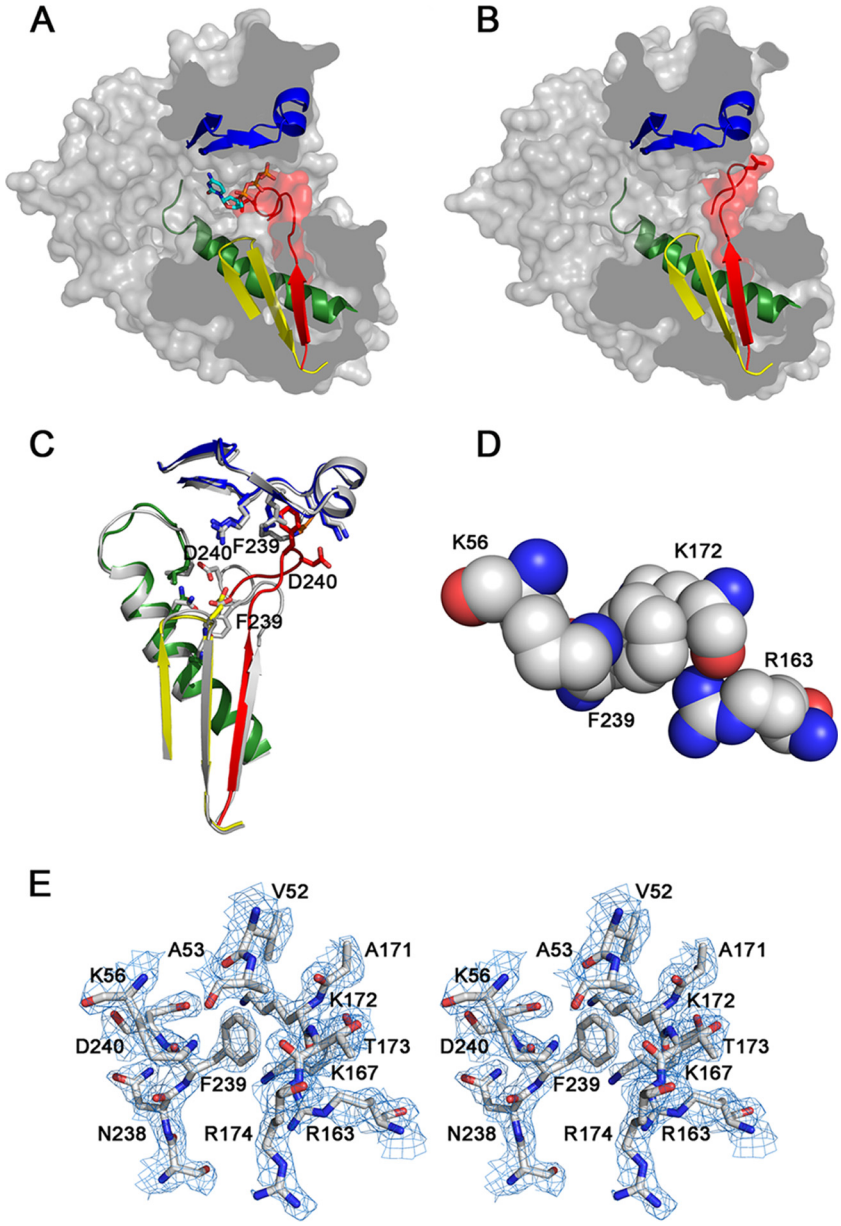

FIG 4 Structural details around the altered conformation of motif A. (A and B) Side views of the RdRp surface representation from C2 (A) and $I4_122$ (B). The surface has been trimmed to expose the three channels through which the different substrates and products of the polymerization reaction enter or leave the active site. The structural elements that support motifs A, B, and C are also shown as ribbons (the colors are the same as those described in the legend to Fig. 2). (C) Structural superimpositions of the C2 (gray) and $I4_122$ structures showing the organization of motifs A, B, C, and F. The amino acids involved in intramolecular contacts stabilizing the two different conformations are shown as sticks. Residues Phe339 and Asp240, showing the largest displacements, are explicitly labeled. (D) Detail of the binding interactions of residue F239. The aromatic ring of Phe239 forms a cation-π interaction with the ε-amino group of the Lys56 side chain and establishes additional interactions with residues Lys172 and Arg163 from motif F. (E) Stereo view of the electron density map around residue Phe239 of motif A. Stereoview of a weighted $2F_o$-F_c Fourier map, contoured at 1.5 σ, with the model placed inside (balls and sticks are colored in atom type code).

site is observed in the $I4_122$ structure (Fig. 2B; also see Fig. 5B). The rearrangement mainly affects the polymerase motif A residues from Tyr236 to Ala246, where Asp240, the amino acid in charge of rNTP selection, and the neighboring Phe239 move ~10 Å away from its position in the catalytic cavity of active RdRp, directed toward the entrance of the nucleotide channel and approaching motif F (Fig. 4B and C). This altered conformation of motif A is mainly stabilized by a cation-π interaction established between the phenyl ring of Phe239 and the ε-amino group of Lys56 located in the finger domain at the C-terminal end of helix α1 (Fig. 4D). The Phe239 side chain is also involved in strong hydrophobic contacts with residues Lys172 and Arg163 in motif F (Fig. 4D and E). Additional interactions contributing to the stabilization of motif A in the altered position are observed between the side chain of residue Thr242 and the finger residue Asn60 and between main and side chains of His243, Leu291, and Asn306

Downloaded from http://jvi.asm.org/ on March 26, 2015 by Universiteitsbibliotheek Utrecht

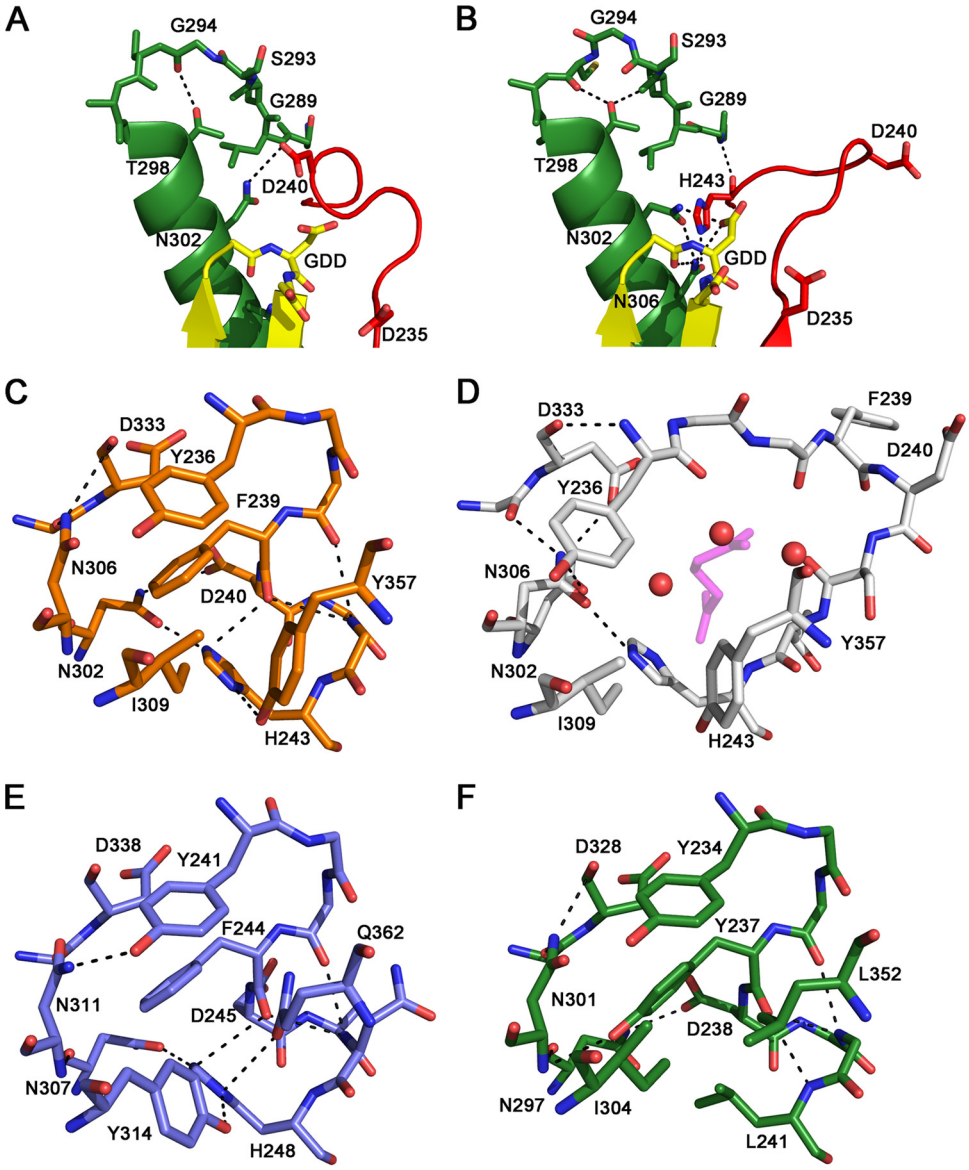

FIG 5 Organization of EMCV 3D^{pol} palm in the two alternative conformations and the Phe239 environment in picornavirus 3D^{pol}. Closeup of the palm subdomain of EMCV 3D^{pol} in the standard (A) and altered (B) conformations, showing the disposition and intramolecular contacts established by the conserved residues Gly289, Ser293, Gly294, and Thr298 within the motif B-loop as well as the interaction between the motif A residue Asp240 and residue Asn302 of motif B, which has been described as essential for rNTP selection. The conserved GDD residues of motif C and the catalytic Asp235 of motif A are also shown and explicitly labeled. (C and D) Structural details around Phe239 in 3D^{pol} of ECMV. When motif A is located in standard conformation (C), His243 interacts with the main-chain oxygen of Phe239, while in the altered conformation (D), the His243 side chain has changed the rotamer and the interaction with F239 is lost. A glutamine present in the buffer fills the new space created by the displacement of the motif. Panels E and F show the same environment in aphthovirus (FMDV; PDB entry 1U09) and enterovirus (PV; PDB entry 1RA6). The structure of the 3D^{pol} of FMDV shows a histidine in the same position as that shown in panel C. Nevertheless, the 3D^{pol} of PV has a Tyr instead of a Phe that interacts with the main chain of Asn297.

within motif B (helix α10) (Fig. 3D). In this altered position of motif A, the active-site residue Asp240 remains totally exposed in the rNTP tunnel edge (Fig. 4B).

The movement of motif A is associated with other conformational changes in the neighboring finger region: from Phe54 to Ser63 (C terminus of the α1 and α1-α2 loop) (Fig. 2B), which directly interacts with motif A in both standard and altered conformations (Fig. 3B, C, and D), and at the 3D^{pol} N terminus, where the very first Gly1 residue moves from its binding site anchored in the finger domain toward a totally exposed orientation in the polymerase surface (Fig. 3D).

In addition, the drastic movement of the motif A loop leaves an empty space in the palm site, particularly where Phe239 used to be packed (Fig. 5C and D). In the structure, this space is filled by the presence of a density which has been interpreted as a glutamine molecule coming from the washing buffer of the concentration filters (see Materials and Methods). A number of water molecules are also found in this region. Finally, the Asn302 and Asn306 side chains have been changed in their rotamer conformation and interact with one another and with Tyr236, partially occupying the Phe239 ring (Fig. 5D).

Structural comparisons have also detected other polymerase

Downloaded from http://jvi.asm.org/ on March 26, 2015 by Universiteitsbibliotheek Utrecht

rearrangements that do not appear to be directly associated with the conformational change of motif A. These movements involve two regions that are essential for polymerase function: the conserved motifs G and D (Fig. 2B and C). Main-chain movements of about 1.8 Å in the region, from Leu99 to Val125, which contains motif G, are observed in comparisons of the $3D^{pol}$ structures belonging to the C2 and $I4_122$ space groups. This region harbors the conserved amino acids Gly112 and Pro114, which have been seen to be involved in template binding and chain translocation by structural and mutational analyses of other picornaviral RdRps (14, 17, 42, 46). In addition, residues from Ile359 to Pro369 within the motif D loop also show substantial flexibility when the polymerases of the two different space groups are compared (RMSD of 3.5 Å) (Fig. 2B).

Evaluation of motif A stability in altered and standard conformations. The knowledge-based potentials of the program Prosa2003 (41) were used to compare the stability of the two different conformations of motif A. These statistical potentials are often used for the selection of a correct protein conformation among a large set of decoys but also to detect stability differences among the structures of various mutants. As the Prosa potentials, calculated for the entire EMCV proteins, indicated that both standard and altered conformations were similarly stable (see Materials and Methods), the analysis was then concentrated in the local disposition of the residues in motif A and on its effect in the closely contacting residues. Therefore, only the flexible stretch of motif A, defined between residues 237 and 243, and the region defined by residues 1 and 50 to 64 were included in the calculations. Mutation scanning was performed, including all possible substitutions within the motif A fragment and the nearest residues, and a new Z-score was calculated for each mutated residue (Table 2). As expected, the scanning showed that most substitutions destabilize the mutant form of the loop in both conformations. However, some positions were stabilized, and most of these stabilizing mutations were found in the standard conformation of the loop (Table 2). Interestingly, among the residues affected by the scanning, Gly1, Lys56, Phe239, and Asp240 are essential for RdRp activity, as has been demonstrated in other picornavirus $3D^{pol}$. Other nonconserved residues within loop A (Ser237 and Ser241) and close to Lys56 (Asp50 and Gln61) also appear to be affected. Another conclusion from the scan is that the scores derived from pair energy are mostly unaffected, proving that the contacts of these residues are quite stable (Table 2). The only position influenced by this scanning is Phe239 in its standard conformation, indicating that the active form of the loop is not the best for a phenylalanine in this position. However, the formation of the π-cation and the relocation of Phe239 in the altered conformation of motif A (Fig. 4C and D) improves the stability of the structure.

According to one of the principles of enzyme catalysis, establishing that an unstable residue tends to stabilize by the interaction with another element (substrate or protein), the analysis of the effect of scanning in the surf energy shows those residues relevant for the reactivity of the protein. Interestingly, both standard and altered conformations show Lys56 destabilized; in contrast, Asp240 appears to be unstable only in the standard conformation, which is indeed the active form of the polymerase.

DISCUSSION

Biochemical analyses of RdRp elongation complexes revealed a multistep model of nucleotide incorporation (47–49). The X-ray structures of various picornaviral replication-elongation complexes, trapped in different steps of the catalytic process, have revealed a mechanism of active-site closure that does not require large interdomain rearrangements (17–20). Structural comparisons evidenced that $3D^{pol}$ uses subtle conformational changes in the palm domain, facilitating the interactions with the ribose hydroxyl groups of the incoming rNTP. In particular, the side chain rearrangements in the conserved aspartic acid of the motif A C terminus (Asp240 in EMCV) and in motif B residues Asn302 and Ser293 are responsible for rNTP recognition and binding (19, 43, 44). Furthermore, a number of basic residues of motif F were also involved in binding the triphosphate moiety of the incoming nucleotide (Fig. 2D and E). After the correct accommodation of the rNTP substrate in the active site, a fine shift of motif A positions the catalytic aspartic acid, located at the N terminus of the motif, in the correct orientation for metal binding (Fig. 2E). A number of catalytic complexes have been crystallized in an initial precatalytic step, where the enzyme shows an open conformation characterized by a partially formed three-stranded β-sheet of the palm domain motifs A and C (17–20) (Fig. 2D). Other elongation complexes were trapped in a catalytically competent closed conformation, where the β-strand structure of motif A was completely formed, allowing catalysis to take place by the common two-metal-ion mechanism (17, 18) (Fig. 2E). These local changes serve to fully structure the active site upon correct nucleotide binding. As picornaviral RdRps do not possess any proofreading activity, the mentioned rearrangements associated with the catalytic cycle seem to be the major fidelity determinants of these enzymes (reviewed in references 50 and 44). Besides these fine movements, recent molecular dynamics and nuclear magnetic resonance data have provided evidence that the motif D loop is highly dynamic and that the movements of this region serve to close the active site when the correct nucleotide is bound (31, 51, 52). This motif contains a strictly conserved lysine, which appears to be the proton donor for the pyrophosphate leaving group after nucleotide incorporation (53). Pyrophosphate protonation is not essential but contributes 50-fold to 1,000-fold to the rate of nucleotide addition (54). Therefore, motif D and, in particular, the dynamics of this conserved lysine appear to comprise an important element affecting both fidelity and polymerization efficiency (31, 51, 53–55).

The six EMCV $3D^{pol}$-independent molecules found in the C2 crystals showed an open conformation of the active site, as expected for the apo-form of the enzyme. In contrast, the $I4_122$ crystals trapped the EMCV enzyme in a closed-like conformation, with the β-sheet supporting motif A totally formed and the catalytic Asp235 positioned in front of the motif C Asp333 (Fig. 4B and C and 5B). This active-site conformation has never been observed before in the absence of RNA and a correctly base-paired NTP. However, the $I4_122$ structure shows an unprecedented movement of the motif A loop harboring the rNTP binding residue Asp240 ~10 Å away from the active site. In this orientation, Asp240 occupies the edge of the NTP entry tunnel (Fig. 4B and C). In addition, all of the residues expected to participate in the EMCV active-site closure during catalysis were involved in contacts stabilizing the altered conformation of the A-loop (Fig. 4C to E). Next to Asp240 is the phenyl ring of Phe239, which forms a π-cation interaction with Lys56 and is further stabilized by hydrophobic interactions with the side chains of Lys172 and Arg173 of motif F (Fig. 4D). Moreover, the main chains of residues Gly290,

Downloaded from http://jvi.asm.org/ on March 26, 2015 by Universiteitsbibliotheek Utrecht

Leu291, Ile310 (motif B), and Asp334 (motif C) also participated in contacts with the altered motif A (Fig. 4D and E). Finally, in this structure the Asp240 interacting residue, Asn302, together with Asn307 appeared hydrogen bonded to the catalytic Asp333 of motif C, which had changed its rotamer conformation (Fig. 5A to D).

The large movement of motif A seems to be associated with other important changes in the molecule. In particular, rearrangements were located at the finger residues 54 to 63 and at the polymerase N terminus. All picornavirus $3D^{pol}$ structures reported to date have shown the N-terminal glycine buried in a pocket at the base of the finger region, participating in a network of hydrogen bonds with other highly conserved glycine residues in finger and palm domains (Fig. 3A and B) (14, 29, 56). This network of interactions helps the correct positioning of the rNTP binding Asp residue in the active site (14). In enterovirus and aphthovirus, the amino group of Gly1 establishes hydrogen bonds with the backbone carbonyls of three conserved glycines, one at the fingers and the last two within the motif B loop, in an almost perfect tetrahedral geometry (Fig. 3A). The conformation was further stabilized by other main-chain hydrogen bonds formed between residues of motifs B and A (Fig. 3B). Previous mutational, biochemical, and structural data on PV showed that the $3D^{pol}$ activity was extremely sensitive to mutations at the N terminus (14, 57, 58). This sensitivity, as well as the lack of polymerase activity in the PV precursor 3CD protein, was thought to be associated with the removal of the $3D^{pol}$ N terminus from its binding pocket and, as a consequence, to an alteration of the pattern of interactions mentioned (29).

In the standard conformation of motif A, Phe239, the amino acid that has experienced the most dramatic rearrangement (Fig. 4 and 5), appears tightly packed to the aromatic residues Tyr236 and His243 within the same motif and makes additional hydrophobic contacts to Ile309 (helix α10 of motif B) and, to a lesser extent, to Tyr357 (motif D loop). In addition, its main-chain oxygen is hydrogen bonded to the His243 side chain, which is also involved in other two polar interactions with the side chains of Asn302 and Tyr357 (Fig. 5C). In the altered structure of motif A, the His243 side chain has changed its rotamer conformation and appears to participate only in a hydrogen bond with the reorganized Asn306 side chain (Fig. 5D). Comparisons to other picornaviral polymerases of known structures demonstrate the high conservation of this palm region (Fig. 5C, E, and F). The equivalent position of Phe239 is always occupied by an aromatic residue in picornaviral polymerases, with Phe in cardiovirus and aphthovirus and Tyr in most enteroviruses. In all of the enterovirus $3D^{pol}$ structures solved, the OH group of this Tyr side chain appears to be hydrogen bonded to a main-chain residue of motif B, being an additional element that stabilizes the motif A loop in the standard conformation (Fig. 5D). The Phe239-interacting residue Tyr236 is also strictly conserved among picornaviruses; however, His234 is only conserved in the cardio- and aphthovirus genera. In FMDV $3D^{pol}$ structures solved, both in absence and in the presence of RNA (19, 20), the equivalent His residue is involved in similar contacts (Fig. 5). In addition, whereas both FMDV and EMCV C2 crystals have been obtained at acidic pH, the EMCV $I4_122$ crystals have grown at pH 8 (19, 20; also see Materials and Methods). Taking into account the different pH conditions used in crystal growth and the pattern of interactions described above, we tentatively speculate that the pH differences affect the protonation state of His243, affecting the interactions mediated by this residue and, as a consequence, preventing or facilitating the large conformational change of the motif A loop. The altered conformation of motif A leaves an empty space in the palm that might be occupied by small molecules, like the glutamine molecule found in the $I4_122$ structure, which probably contribute to the stabilization of this altered conformation.

In conclusion, the structural data presented here suggest that the motif A loop would act as a negative regulator of RNA synthesis, interfering with the access of the incoming nucleotides to the active site. The role of this negative regulation is not known. However, the participation of highly conserved residues in maintaining the altered form of motif A, especially in cardio- and aphthoviruses, suggests that this conformational change is general at least to the polymerases of these two picornavirus genera. The presence of flexible elements in the polymerase regions that play roles in template, primer, or nucleotide binding is essential for its function. The dynamics of these elements can be modulated by external effectors, either activating or inhibiting the enzyme activity. Small-molecule compounds designed to stabilize altered motif A would prevent the correct positioning of the incoming rNTP to the active site and, as a consequence, the polymerization function in picornaviruses.

ACKNOWLEDGMENTS

We thank J. Querol-Audí for revising the manuscript and the Plataforma Automatitzada de Cristallografia (Barcelona) for technical assistance in the initial crystallization screenings.

This work was supported by research grants from the SILVER Large Scale Collaborative Project (grant agreement number 260644) of the European Union 7th Framework (B.C., F.J.M.V.K., and N.V.) and from the Spanish Ministry of Economy and Competitivity, BIO2011-24333 (N.V.). L.V.-A. is supported by an FI fellowship from AGAUR. C.F.-O. is the recipient of a JAE postdoctoral contract from CSIC, cofinanced by Fondo Social Europeo.

X-ray data were collected at the Xaloc beamline at the ALBA Synchrotron Light Facility with the collaboration of Fernando Gil.

REFERENCES

1. **Norder H, De Palma AM, Selisko B, Costenaro L, Papageorgiou N, Arnan C, Coutard B, Lantez V, De Lamballerie X, Baronti C, Sola M, Tan J, Neyts J, Canard B, Coll M, Gorbalenya AE, Hilgenfeld R.** 2011. Picornavirus non-structural proteins as targets for new anti-virals with broad activity. Antiviral Res. **89:**204–218. http://dx.doi.org/10.1016/j.antiviral.2010.12.007.
2. **Knowles NJ, Hovi T, King AMQ, Stanway G.** 2010. Overview of taxonomy, p 19–32. *In* Ehrenfeld E, Domingo E, Roos RP (ed), The picornaviruses. American Society for Microbiology, Washington, DC.
3. **Duke GM, Hoffman MA, Palmenberg AC.** 1992. Sequence and structural elements that contribute to efficient encephalomyocarditis virus RNA translation. J. Virol. **66:**1602–1609.
4. **Brahic M, Bureau JF, Michiels T.** 2005. The genetics of the persistent infection and demyelinating disease caused by Theiler's virus. Annu. Rev. Microbiol. **59:**279–298. http://dx.doi.org/10.1146/annurev.micro.59.030804.121242.
5. **Ohsawa K, Watanabe Y, Miyata H, Sato H.** 2003. Genetic analysis of a Theiler-like virus isolated from rats. Comp. Med. **53:**191–196. http://www.ncbi.nlm.nih.gov/pubmed/12784854.
6. **Pritchard AE, Strom T, Lipton HL.** 1992. Nucleotide sequence identifies Vilyuisk virus as a divergent Theiler's virus. Virology **191:**469–472. http://dx.doi.org/10.1016/0042-6822(92)90212-8.
7. **Zimmerman JJ.** 1994. Encephalomyocarditis, p 423–436. *In* Beran GW, Steele JH (ed), CRC handbook series in zoonoses. CRC Press, Boca Raton, FL.
8. **Himeda T, Ohara Y.** 2012. Saffold virus, a novel human Cardiovirus with unknown pathogenicity. J. Virol. **86:**1292–1296. http://dx.doi.org/10.1128/JVI.06087-11.
9. **Jones MS, Lukashov VV, Ganac RD, Schnurr DP.** 2007. Discovery of a novel human picornavirus in a stool sample from a pediatric patient presenting with fever of unknown origin. J. Clin. Microbiol. **45:**2144–2150. http://dx.doi.org/10.1128/JCM.00174-07.

Downloaded from http://jvi.asm.org/ on March 26, 2015 by Universiteitsbibliotheek Utrecht

10. **Liang Z, Kumar AS, Jones MS, Knowles NJ, Lipton HL.** 2008. Phylogenetic analysis of the species Theilovirus: emerging murine and human pathogens. J. Virol. **82:**11545–11554. http://dx.doi.org/10.1128/JVI.01160-08.
11. **Blinkova O, Rosario K, Li L, Kapoor A, Slikas B, Bernardin F, Breitbart M, Delwart E.** 2009. Frequent detection of highly diverse variants of cardiovirus, cosavirus, bocavirus, and circovirus in sewage samples collected in the United States. J. Clin. Microbiol. **47:**3507–3513. http://dx.doi.org/10.1128/JCM.01062-09.
12. **Zoll J, Erkens Hulshof S, Lanke K, Verduyn Lunel F, Melchers WJ, Schoondermark-van de Ven E, Roivainen M, Galama JM, van Kuppeveld FJ.** 2009. Saffold virus, a human Theiler's-like cardiovirus, is ubiquitous and causes infection early in life. PLoS Pathog. **5:**e1000416. http://dx.doi.org/10.1371/journal.ppat.1000416.
13. **Wu Y, Lou Z, Miao Y, Yu Y, Dong H, Peng W, Bartlam M, Li X, Rao Z.** 2010. Structures of EV71 RNA-dependent RNA polymerase in complex with substrate and analogue provide a drug target against the hand-foot-and-mouth disease pandemic in China. Protein Cell. **1:**491–500. http://dx.doi.org/10.1007/s13238-010-0061-7.
14. **Thompson AA, Peersen OB.** 2004. Structural basis for proteolysis-dependent activation of the poliovirus RNA-dependent RNA polymerase. EMBO J. **23:**3462–3471. http://dx.doi.org/10.1038/sj.emboj.7600357.
15. **Love RA, Maegley KA, Yu X, Ferre RA, Lingardo LK, Diehl W, Parge HE, Dragovich PS, Fuhrman SA.** 2004. The crystal structure of the RNA-dependent RNA polymerase from human rhinovirus: a dual function target for common cold antiviral therapy. Structure **12:**1533–1544. http://dx.doi.org/10.1016/j.str.2004.05.024.
16. **Gruez A, Selisko B, Roberts M, Bricogne G, Bussetta C, Jabafi I, Coutard B, De Palma AM, Neyts J, Canard B.** 2008. The crystal structure of coxsackievirus B3 RNA-dependent RNA polymerase in complex with its protein primer VPg confirms the existence of a second VPg binding site on Picornaviridae polymerases. J. Virol. **82:**9577–9590. http://dx.doi.org/10.1128/JVI.00631-08.
17. **Gong P, Peersen OB.** 2010. Structural basis for active site closure by the poliovirus RNA-dependent RNA polymerase. Proc. Natl. Acad. Sci. U. S. A. **107:**22505–22510. http://dx.doi.org/10.1073/pnas.1007626107.
18. **Gong P, Kortus MG, Nix JC, Davis RE, Peersen OB.** 2013. Structures of coxsackievirus, rhinovirus, and poliovirus polymerase elongation complexes solved by engineering RNA mediated crystal contacts. PLoS One **8:**e60272. http://dx.doi.org/10.1371/journal.pone.0060272.
19. **Ferrer-Orta C, Arias A, Perez-Luque R, Escarmis C, Domingo E, Verdaguer N.** 2007. Sequential structures provide insights into the fidelity of RNA replication. Proc. Natl. Acad. Sci. U. S. A. **104:**9463–9468. http://dx.doi.org/10.1073/pnas.0700518104.
20. **Ferrer-Orta C, Arias A, Perez-Luque R, Escarmis C, Domingo E, Verdaguer N.** 2004. Structure of foot-and-mouth disease virus RNA-dependent RNA polymerase and its complex with a template-primer RNA. J. Biol. Chem. **279:**47212–47221. http://dx.doi.org/10.1074/jbc.M405465200.
21. **Ferrer-Orta C, Arias A, Agudo R, Perez-Luque R, Escarmis C, Domingo E, Verdaguer N.** 2006. The structure of a protein primer-polymerase complex in the initiation of genome replication. EMBO J. **25:**880–888. http://dx.doi.org/10.1038/sj.emboj.7600971.
22. **Campagnola G, Weygandt M, Scoggin K, Peersen O.** 2008. Crystal structure of coxsackievirus B3 3Dpol highlights the functional importance of residue 5 in picornavirus polymerases. J. Virol. **82:**9458–9464. http://dx.doi.org/10.1128/JVI.00647-08.
23. **Appleby TC, Luecke H, Shim JH, Wu JZ, Cheney IW, Zhong W, Vogeley L, Hong Z, Yao N.** 2005. Crystal structure of complete rhinovirus RNA polymerase suggests front loading of protein primer. J. Virol. **79:**277–288. http://dx.doi.org/10.1128/JVI.79.1.277-288.2005.
24. **Ferrer-Orta C, Verdaguer N.** 2009. RNA virus polymerases, p 383–401. *In* Cameron CE, Götte M, Raney KD (ed), Viral genome replication. Springer, New York, NY.
25. **Garriga D, Ferrer-Orta C, Querol-Audi J, Oliva B, Verdaguer N.** 2013. Role of motif B loop in allosteric regulation of RNA-dependent RNA polymerization activity. J. Mol. Biol. **425:**2279–2287. http://dx.doi.org/10.1016/j.jmb.2013.03.034.
26. **Pfeiffer JK, Kirkegaard K.** 2003. A single mutation in poliovirus RNA-dependent RNA polymerase confers resistance to mutagenic nucleotide analogs via increased fidelity. Proc. Natl. Acad. Sci. U. S. A. **100:**7289–7294. http://dx.doi.org/10.1073/pnas.1232294100.
27. **Arnold JJ, Vignuzzi M, Stone JK, Andino R, Cameron CE.** 2005. Remote site control of an active site fidelity checkpoint in a viral RNA-dependent RNA polymerase. J. Biol. Chem. **280:**25706–25716. http://dx.doi.org/10.1074/jbc.M503444200.
28. **Agudo R, Ferrer-Orta C, Arias A, de la Higuera I, Perales C, Perez-Luque R, Verdaguer N, Domingo E.** 2010. A multi-step process of viral adaptation to a mutagenic nucleoside analogue by modulation of transition types leads to extinction-escape. PLoS Pathog. **6:**e1001072. http://dx.doi.org/10.1371/journal.ppat.1001072.
29. **Marcotte LL, Wass AB, Gohara DW, Pathak HB, Arnold JJ, Filman DJ, Cameron CE, Hogle JM.** 2007. Crystal structure of poliovirus 3CD protein: virally encoded protease and precursor to the RNA-dependent RNA polymerase. J. Virol. **81:**3583–3596. http://dx.doi.org/10.1128/JVI.02306-06.
30. **Ferrer-Orta C, Sierra M, Agudo R, de la Higuera I, Arias A, Perez-Luque R, Escarmis C, Domingo E, Verdaguer N.** 2010. Structure of foot-and-mouth disease virus mutant polymerases with reduced sensitivity to ribavirin. J. Virol. **84:**6188–6199. http://dx.doi.org/10.1128/JVI.02420-09.
31. **Moustafa IM, Shen H, Morton B, Colina CM, Cameron CE.** 2011. Molecular dynamics simulations of viral RNA polymerases link conserved and correlated motions of functional elements to fidelity. J. Mol. Biol. **410:**159–181. http://dx.doi.org/10.1016/j.jmb.2011.04.078.
32. **Shen H, Sun H, Li G.** 2012. What is the role of motif D in the nucleotide incorporation catalyzed by the RNA-dependent RNA polymerase from poliovirus? PLoS Comput. Biol. **8:**e1002851. http://dx.doi.org/10.1371/journal.pcbi.1002851.
33. **Duke GM, Palmenberg AC.** 1989. Cloning and synthesis of infectious cardiovirus RNAs containing short, discrete poly(C) tracts. J. Virol. **63:**1822–1826.
34. **Lantez V, Dalle K, Charrel R, Baronti C, Canard B, Coutard B.** 2011. Comparative production analysis of three phlebovirus nucleoproteins under denaturing or non-denaturing conditions for crystallographic studies. PLoS Negl. Trop. Dis. **5:**e936. http://dx.doi.org/10.1371/journal.pntd.0000936.
35. **Kabsch W.** 2010. Xds. Acta Crystallogr. D Biol. Crystallogr. **66**(Part 2):125–132. http://dx.doi.org/10.1107/S0907444909047337.
36. **Potterton E, Briggs P, Turkenburg M, Dodson E.** 2003. A graphical user interface to the CCP4 program suite. Acta Crystallogr. D Biol. Crystallogr. **59**(Part 7):1131–1137. http://dx.doi.org/10.1107/S0907444903008126.
37. **Adams PD, Afonine PV, Bunkoczi G, Chen VB, Davis IW, Echols N, Headd JJ, Hung LW, Kapral GJ, Grosse-Kunstleve RW, McCoy AJ, Moriarty NW, Oeffner R, Read RJ, Richardson DC, Richardson JS, Terwilliger TC, Zwart PH.** 2010. PHENIX: a comprehensive Python-based system for macromolecular structure solution. Acta Crystallogr. D Biol. Crystallogr. **66**(Part 2):213–221. http://dx.doi.org/10.1107/S0907444909052925.
38. **Emsley P, Lohkamp B, Scott WG, Cowtan K.** 2010. Features and development of Coot. Acta Crystallogr. D Biol. Crystallogr. **66**(Part 4):486–501. http://dx.doi.org/10.1107/S0907444910007493.
39. **Murshudov GN, Vagin AA, Dodson EJ.** 1997. Refinement of macromolecular structures by the maximum-likelihood method. Acta Crystallogr. D Biol. Crystallogr. **53**(Part 3):240–255. http://dx.doi.org/10.1107/S0907444996012255.
40. **Golovanov AP, Hautbergue GM, Wilson SA, Lian LY.** 2004. A simple method for improving protein solubility and long-term stability. J. Am. Chem. Soc. **126:**8933–8939. http://dx.doi.org/10.1021/ja049297h.
41. **Wiederstein M, Sippl MJ.** 2007. ProSA-web: interactive web service for the recognition of errors in three-dimensional structures of proteins. Nucleic Acids Res. **35:**W407–W410. http://dx.doi.org/10.1093/nar/gkm290.
42. **Arias A, Agudo R, Ferrer-Orta C, Perez-Luque R, Airaksinen A, Brocchi E, Domingo E, Verdaguer N, Escarmis C.** 2005. Mutant viral polymerase in the transition of virus to error catastrophe identifies a critical site for RNA binding. J. Mol. Biol. **353:**1021–1032. http://dx.doi.org/10.1016/j.jmb.2005.09.022.
43. **Ferrer-Orta C, Agudo R, Domingo E, Verdaguer N.** 2009. Structural insights into replication initiation and elongation processes by the FMDV RNA-dependent RNA polymerase. Curr. Opin. Struct. Biol. **19:**752–758. http://dx.doi.org/10.1016/j.sbi.2009.10.016.
44. **Lescar J, Canard B.** 2009. RNA-dependent RNA polymerases from flaviviruses and Picornaviridae. Curr. Opin. Struct. Biol. **19:**759–767. http://dx.doi.org/10.1016/j.sbi.2009.10.011.
45. **Dmitrieva TM, Alexeevski AV, Shatskaya GS, Tolskaya EA, Gmyl AP, Khitrina EV, Agol VI.** 2007. Significance of the C-terminal amino acid residue in mengovirus RNA-dependent RNA polymerase. Virology **365:**79–91. http://dx.doi.org/10.1016/j.virol.2007.02.038.
46. **Kortus MG, Kempf BJ, Haworth KG, Barton DJ, Peersen OB.** 2012. A

Downloaded from http://jvi.asm.org/ on March 26, 2015 by Universiteitsbibliotheek Utrecht

template RNA entry channel in the fingers domain of the poliovirus polymerase. J. Mol. Biol. **417:**263–278. http://dx.doi.org/10.1016/j.jmb.2012.01.049.
47. **Gohara DW, Crotty S, Arnold JJ, Yoder JD, Andino R, Cameron CE.** 2000. Poliovirus RNA-dependent RNA polymerase (3Dpol): structural, biochemical, and biological analysis of conserved structural motifs A and B. J. Biol. Chem. **275:**25523–25532. http://dx.doi.org/10.1074/jbc.M002671200.
48. **Gohara DW, Arnold JJ, Cameron CE.** 2004. Poliovirus RNA-dependent RNA polymerase (3Dpol): kinetic, thermodynamic, and structural analysis of ribonucleotide selection. Biochemistry **43:**5149–5158. http://dx.doi.org/10.1021/bi035429s.
49. **Arnold JJ, Gohara DW, Cameron CE.** 2004. Poliovirus RNA-dependent RNA polymerase (3Dpol): pre-steady-state kinetic analysis of ribonucleotide incorporation in the presence of Mn2+. Biochemistry **43:**5138–5148. http://dx.doi.org/10.1021/bi035213q.
50. **Castro C, Arnold JJ, Cameron CE.** 2005. Incorporation fidelity of the viral RNA-dependent RNA polymerase: a kinetic, thermodynamic and structural perspective. Virus Res. **107:**141–149. http://dx.doi.org/10.1016/j.virusres.2004.11.004.
51. **Yang X, Smidansky ED, Maksimchuk KR, Lum D, Welch JL, Arnold JJ, Cameron CE, Boehr DD.** 2012. Motif D of viral RNA-dependent RNA polymerases determines efficiency and fidelity of nucleotide addition. Structure **20:**1519–1527. http://dx.doi.org/10.1016/j.str.2012.06.012.
52. **Shen H, Moustafa IM, Cameron CE, Colina CM.** 2012. Exploring the dynamics of four RNA-dependent RNA polymerases by a coarse-grained model. J. Phys. Chem. B **116:**14515–14524. http://dx.doi.org/10.1021/jp302709v.
53. **Castro C, Smidansky ED, Arnold JJ, Maksimchuk KR, Moustafa IM, Uchida A, Götte M, Konigsberg W, Cameron CE.** 2009. Nucleic acid polymerases use a general acid for nucleotidyl transfer. Nat. Struct. Mol. Biol. **16:**212–218. http://dx.doi.org/10.1038/nsmb.1540.
54. **Castro C, Smidansky E, Maksimchuk KR, Arnold JJ, Korneeva VS, Gotte M, Konigsberg W, Cameron CE.** 2007. Two proton transfers in the transition state for nucleotidyl transfer catalyzed by RNA- and DNA-dependent RNA and DNA polymerases. Proc. Natl. Acad. Sci. U. S. A. **104:**4267–4272. http://dx.doi.org/10.1073/pnas.0608952104.
55. **Verdaguer N, Ferrer-Orta C.** 2012. Conformational changes in motif D of RdRps as fidelity determinant. Structure **20:**1448–1450. http://dx.doi.org/10.1016/j.str.2012.08.014.
56. **Ferrer-Orta C, Arias A, Escarmis C, Verdaguer N.** 2006. A comparison of viral RNA-dependent RNA polymerases. Curr. Opin. Struct. Biol. **16:**27–34. http://dx.doi.org/10.1016/j.sbi.2005.12.002.
57. **Hobson SD, Rosenblum ES, Richards OC, Richmond K, Kirkegaard K, Schultz SC.** 2001. Oligomeric structures of poliovirus polymerase are important for function. EMBO J. **20:**1153–1163. http://dx.doi.org/10.1093/emboj/20.5.1153.
58. **Rothstein MA, Richards OC, Amin C, Ehrenfeld E.** 1988. Enzymatic activity of poliovirus RNA polymerase synthesized in Escherichia coli from viral cDNA. Virology **164:**301–308. http://dx.doi.org/10.1016/0042-6822(88)90542-9.
59. **Sippl MJ.** 1993. Recognition of errors in three-dimensional structures of proteins. Proteins **17:**355–362. http://dx.doi.org/10.1002/prot.340170404.
60. **Aloy P, Oliva B.** 2009. Splitting statistical potentials into meaningful scoring functions: testing the prediction of near-native structures from decoy conformations. BMC Struct. Biol. **9:**71. http://dx.doi.org/10.1186/1472-6807-9-71.
61. **Marti-Renom MA, Madhusudhan MS, Fiser A, Rost B, Sali A.** 2002. Reliability of assessment of protein structure prediction methods. Structure **10:**435–440. http://dx.doi.org/10.1016/S0969-2126(02)00731-1.
62. **Sippl MJ.** 1990. Calculation of conformational ensembles from potentials of mean force. An approach to the knowledge-based prediction of local structures in globular proteins. J. Mol. Biol. **213:**859–883.

Downloaded from http://jvi.asm.org/ on March 26, 2015 by Universiteitsbibliotheek Utrecht